ASIAN JOURNAL OF CIVIL ENGINEERING (BUILDING AND HOUSING) VOL. 11, NO. 5 (2010)
PAGES 605-626

# THREE-DIMENSIONAL SCATTERING OF PLANE HARMONIC SH, SV, AND P WAVES IN MULTILAYERED ALLUVIAL VALLEYS

B. Omidvar[a]*, M. Rahimian[b], T. Mohammadnejad[c] and A. Sanaeiha[b]
[a]Faculty of Environment, University of Tehran, 14155-6135 Tehran, Iran
[b]Faculty of Civil Engineering, University of Tehran, Tehran, Iran
[c]Department of Civil Engineering, Sharif University of Technology, Tehran, Iran

## ABSTRACT

In this paper, three-dimensional amplification of plane harmonic SH, SV, and P waves in multilayered alluvial valleys is investigated by using a boundary element method in frequency domain. It is shown that in order to achieve real responses, the problem must be analyzed and modeled three-dimensionally. Also, for exact evaluation of surface ground motions in alluvial valleys all key parameters such as layering, material and geometrical characteristics of each layer, stimulation frequency, wave type, plus angle and azimuth of incidence must be taken into account altogether.

The accuracy and efficiency of the proposed formulations for the computation of the surface displacement field amplification is verified by solving a number of problems.

**Keywords:** Boundary element method; wave propagation; site effects; multilayered alluvial valley; 3D models

## 1. INTRODUCTION

The study of topographic effects and sediments on amplification of earthquake waves has been the main subject of various studies. In the recent years, the importance of site effects in the local amplification of surface ground motion has been well recognized. Study of ground motions in topographies and basins needs three-dimensional modeling because of numerous reasons. The response of a 3D topography depends on the angle, azimuth and type of incident wave. Lateral variations of the sediment thickness could cause interaction of the alluvial layers to be dependent on the azimuth of the wave. In addition, the 3D curvature of the alluvium-basement interface could cause focusing of body waves for certain locations in the basin. These have led a number of researchers to study more realistic problems. Most of the published papers in this field are limited to simple geometries and axisymmetric cases. Sanchez-Sesma [1] considered diffraction of a vertical incident P wave by several types of

* E-mail address of the corresponding author: bomidvar@ut.ac.ir (B. Omidvar)

irregularities including canyon and alluvial basins using the c-complete family of wave functions. This study was limited to axisymmetric cases. Lee and Langston [2] investigated the wave propagation in a three-dimensional circular basin subjected to incident plane P and SH waves using a ray technique. Their solution was applicable only in the high frequency range. Lee [3] extended the method to study the case of a hemispherical alluvial valley, but his solution is applicable for irregularities of spherical shape only. Eshraghi and Dravinski [4] studied a non-symmetric model for P-, S- and Rayleigh waves also for alluvial valleys. Sanchez-Sesma et al. [5] investigated the response of an axisymmetric alluvial valley for incident SH-waves. Sanchez-Sesma et al. [6] obtained the polarization of waves for a cylindrical deposit.

Some works have been done to study the 3D scattering from two-dimensional (2D) structures. Luco et al. [7] used an indirect boundary method to obtain the response of an infinitely long canyon of uniform, but arbitrary cross-section, in a viscoelastic layered half space, for incident P- and S- waves. Zhang and Chopra [8] investigated the same problem using the direct boundary element method for a homogeneous half-space including Rayleigh waves. The time-harmonic response of uniform, circular cylindrical valleys of semi-circular and semi-elliptical cross-section embedded in a uniform half-space using a combination of the boundary element method and the finite element method has been proposed for P, SV, SH and Rayleigh waves by Khair et al. [9-10]. Liu et al. [11] studied scattering of obliquely incident seismic waves by a cylindrical valley in a layered half-space using the combination of the finite and boundary element methods.

The study of 3D alluvial valleys has been subject of other researches. Yomogida and Etgen [12] also used the finite-difference method to study the Los Angeles basin for the Whittier-Narrows earthquake. Hizada et al. [13] obtained 3-D simulations of surface wave propagation in the Kanto sedimentary basin. Later, Sanchez-Sesma et al. [14-15] studied wave amplification in three-dimensional alluvial valleys. Other numerical results were reported by Barros and Luco [16] to illustrate the time-harmonic, three-dimensional response of cylindrical valleys embedded in uniform and layered media under obliquely incident P and S waves. Scattering of plane harmonic waves by multiple dipping layers was conducted by Dravinski and Mossessian [17]. Mossessian and Dravinski [18] have also applied an indirect boundary integral equation method to study amplification of elastic waves by three-dimensional canyons of arbitrary shape. Reinoso et al. [19] have presented a direct boundary element method for calculating the three-dimensional scattering of seismic waves from irregular topographies and buried valleys due to incident P-, S- and Rayleigh waves. Mohammadnejad [20] has studied 3-D topographic effects and basins on amplification of earthquake waves. Gatmiri and Arson [21-22] have studied Seismic site effects by an optimized 2D BE/FE method. Lee et al. [23] have demonstrated Effects of Topography on Seismic-Wave Propagation by developing a new spectral-element mesh implementation to accommodate realistic topography. Recently, Rahimian et al. [24] have studied effects of arbitrary shaped surface topographies on earthquake ground motion using BEM in time domain. Because of the complexity of the problems in reality, closed form analytical solutions are not accessible for them. However, latest advances in computational techniques have made numerical approaches more practical for realistic problems. Boundary element method (BEM) is one of such approaches. This technique formulates the problem in

terms of boundary values. The main advantage of BEM, especially in comparison with finite element and finite difference methods, is that the discretization is only applied to the boundary, thus reducing the volume of modeling and the number of unknown variables. Moreover, the radiation condition at infinity is exactly satisfied in this method which is very striking for wave propagation problems.

In this study, the BEM in frequency domain is employed. The accuracy of the present method is tested through comparison with results of some earlier studies. Numerical results for several multilayered alluvial valleys are presented. Influence of mechanical properties of sedimentary layers, dimensionless frequency of incident wave, soil layering, thickness of sedimentary layers and number of layers is investigated.

## 2. PROPAGATION OF PLANE HARMONIC WAVES IN A HALF-SPACE

Consider $\Omega$ as a homogeneous and linearly elastic three-dimensional half-space under the boundary $\Gamma$ at $\mathbf{y} = \mathbf{0}$. The propagation of plane harmonic waves in domain $\Omega$ is described by the Navier-Cauchy equation. For time-harmonic problems, with the dependence on time as $\exp(\mathbf{i\omega\, t})$, the Navier-Cauchy equation is as follows

$$\mathbf{c}_2^2\nabla^2\mathbf{u} + (\mathbf{c}_1^2 - \mathbf{c}_2^2)\nabla(\nabla.\mathbf{u}) + \boldsymbol{\omega}^2\mathbf{u} = \mathbf{0} \tag{1}$$

where

$$\mathbf{c}_1 = \left(\frac{\boldsymbol{\lambda} + \mathbf{2\mu}}{\boldsymbol{\rho}}\right)^{1/2} \;;\; \mathbf{c}_2 = \left(\frac{\boldsymbol{\mu}}{\boldsymbol{\rho}}\right)^{1/2} \tag{2}$$

are the longitudinal and transversal wave velocities, respectively. $\omega$ is the circular frequency of the incident wave and u is the displacement vector. The solution of the Navier-Cauchy equation has to satisfy the traction-free boundary condition at the boundary $\Gamma$.

One method of solving equation (1) is to use potential functions. According to Helmholtz theorem, the displacement field **u** can be expressed as the sum of the gradient of a scalar field $\varphi$, plus the curl of a vector field $\psi$, i.e.

$$\mathbf{u} = \nabla\varphi + \nabla\times\boldsymbol{\psi} \tag{3}$$

$\psi$ must be such that the relation $\nabla.\boldsymbol{\psi} = 0$ is satisfied. The displacement field in the form of equation (3) satisfies the Navier-Cauchy equation if the potential functions satisfy the following equations

$$\begin{aligned} \nabla^2\varphi \;+\; k_1^2\,\varphi \;&= 0 \\ \nabla^2\psi_k + k_2^2\,\psi_k &= 0 \end{aligned} \tag{4}$$

with $\mathrm{k}_1 = \omega/\mathrm{c}_1$ and $\mathrm{k}_2 = \omega/\mathrm{c}_2$ the longitudinal and transversal wave numbers, respectively. Equations (4) are called the Helmholtz equations or the wave equations in the frequency domain (reduced wave equations).

Assume that the plane waves travel in the $x'-y'$ plane, so it is yielded $\partial/\partial z'=0$. By using the Helmholtz decomposition, the in-plane displacements $u'$ and $v'$ are given as

$$\begin{aligned} u' &= \frac{\partial \varphi}{\partial x'} + \frac{\partial \psi}{\partial y'} \\ v' &= \frac{\partial \varphi}{\partial y'} - \frac{\partial \psi}{\partial x'} \end{aligned} \tag{5}$$

while the out-of-plane displacement $\omega'$ is as follows

$$\omega' = \frac{\partial \psi_2}{\partial x'} - \frac{\partial \psi_1}{\partial y'} \tag{6}$$

Consider the reference coordinate system $x, y, z$. In the general case that normal to the wave front, i.e. the wave propagation direction, lies in the $x'-y'(y'=y)$ plane (Figure 1) where the $x'-z'$ plane forms a horizontal incidence angle $\theta_h$ with respect to the general plane $x-z$, the displacements in the general system are obtained by using the following transformation matrix as follows

$$\begin{Bmatrix} u \\ v \\ \omega \end{Bmatrix} = \begin{bmatrix} \cos\theta_h & 0 & -\sin\theta_h \\ 0 & 1 & 0 \\ \sin\theta_h & 0 & \cos\theta_h \end{bmatrix} \begin{Bmatrix} u' \\ v' \\ \omega' \end{Bmatrix} = \mathbf{T} \begin{Bmatrix} u' \\ v' \\ \omega' \end{Bmatrix} \tag{7}$$

Also, we have the following relations

$$\begin{aligned} x' &= x\cos\theta_h + z\sin\theta_h \\ y' &= y \end{aligned} \tag{8}$$

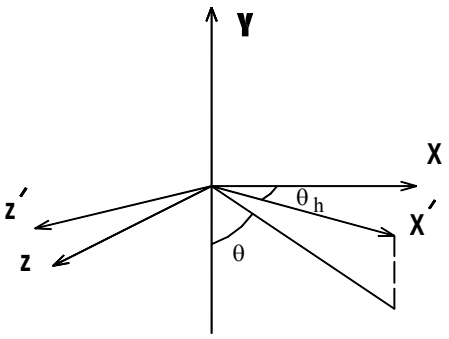


Figure 1. Position of the propagation wave plane $x'-y'(y'=y)$ relative to the reference coordinate system $x-y-z$

*2.1 Incident SH wave*

The solution at any point in the half-space is given by the sum of $\omega_I$, the incident SH wave, and $\omega_R$, the reflected SH wave (Figure 2a):

$$\begin{aligned} \omega_I &= C_\circ \exp\{-ik_2(x'\sin\theta_3 + y'\cos\theta_3)\} \\ \omega_R &= C_\circ \exp\{-ik_2(x'\sin\theta_3 - y'\cos\theta_3)\} \end{aligned} \tag{9}$$

where $\theta_3$ is the incidence angle with respect to the y-axis, and $C_o$ is the incident wave amplitude. The displacement field $\mathbf{u_o}$ is given by

$$\mathbf{u}_\mathbf{o} = \begin{Bmatrix} u \\ v \\ \omega \end{Bmatrix} = \mathbf{T} \begin{Bmatrix} 0 \\ 0 \\ \omega_I + \omega_R \end{Bmatrix} \tag{10}$$

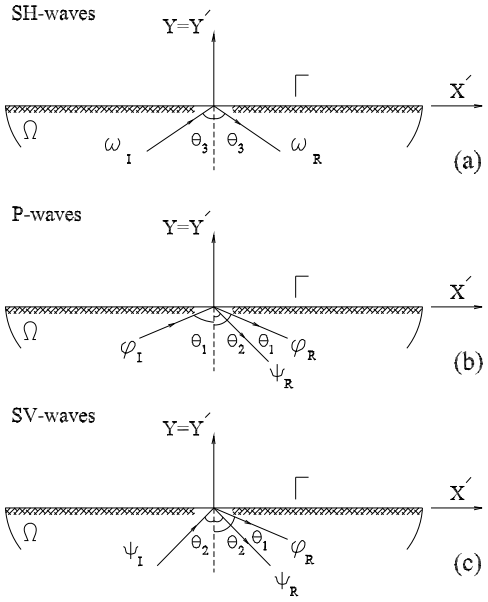


Figure 2. Incidence and reflection of waves in half-space

*2.2 Incident P wave*

The solution at any point in the half-space is given by the combination of $\varphi_I$, the incident P wave, and $\varphi_R$ and $\psi_R$, the reflected P and SV waves, respectively (Figure 2b):

$$\begin{aligned} \varphi_I &= A_o \exp\{-ik_1(x'\sin\theta_1 + y'\cos\theta_1)\} \\ \varphi_R &= A_1 \exp\{-ik_1(x'\sin\theta_1 - y'\cos\theta_1)\} \\ \psi_R &= B_1 \exp\{-ik_2(x'\sin\theta_2 - y'\cos\theta_2)\} \end{aligned} \tag{11}$$

where $\theta_1$ is the incidence angle relative to the y-axis, and $A_o$ is the incident wave amplitude. The angle of the reflected SV wave relative to the vertical axis is given by $\theta_2 = \sin^{-1}(k^{-1}\sin\theta_1)$, where $k = c_1/c_2 = \{2(1-\nu)/(1-2\nu)\}^{1/2}$ is the material constant. The amplitude ratios are defined by

$$\frac{A_1}{A_o} = \frac{\sin 2\theta_1 \sin 2\theta_2 - k^2 \cos^2 2\theta_2}{\sin 2\theta_1 \sin 2\theta_2 + k^2 \cos^2 2\theta_2}$$
$$\frac{B_1}{A_o} = \frac{-2k \sin 2\theta_1 \cos 2\theta_2}{\sin 2\theta_1 \sin 2\theta_2 + k^2 \cos^2 2\theta_2} \tag{12}$$

The displacement field $\mathbf{u_o}$ is as follows

$$\mathbf{u_o} = \begin{Bmatrix} u \\ v \\ \omega \end{Bmatrix} = \mathbf{T} \begin{Bmatrix} \sin\theta_1(-\varphi_I - \varphi_R) + \cos\theta_2 \psi_R \\ \cos\theta_1(-\varphi_I + \varphi_R) + \sin\theta_2 \psi_R \\ 0 \end{Bmatrix} \times ik_1 \tag{13}$$

*2.3 Incident SV wave*

The solution at any point in the half-space is obtained through the combination of $\psi_I$, the incident SV wave, and $\psi_R$ and $\varphi_R$, the reflected SV and P waves, respectively (Figure 2c):

$$\psi_I = B_o \exp\{-ik_2(x'\sin\theta_2 + y'\cos\theta_2)\}$$
$$\psi_R = B_1 \exp\{-ik_2(x'\sin\theta_2 - y'\cos\theta_2)\}$$
$$\varphi_R = A_1 \exp\{-ik_1(x'\sin\theta_1 - y'\cos\theta_1)\} \tag{14}$$

where $\theta_2$ is the angle of the incident SV wave with respect to the y-axis, and $B_o$ is the incident wave amplitude. The reflection angle of the P wave relative to the vertical axis is defined by $\theta_1 = \sin^{-1}(k\sin\theta_2)$. The reflection coefficients are specified by

$$\frac{B_1}{B_o} = \frac{\sin 2\theta_1 \sin 2\theta_2 - k^2 \cos^2 2\theta_2}{\sin 2\theta_1 \sin 2\theta_2 + k^2 \cos^2 2\theta_2}$$
$$\frac{A_1}{B_o} = \frac{k \sin 4\theta_2}{\sin 2\theta_1 \sin 2\theta_2 + k^2 \cos^2 2\theta_2} \tag{15}$$

The displacement field $\mathbf{u_o}$ is given by

$$\mathbf{u_o} = \begin{Bmatrix} u \\ v \\ \omega \end{Bmatrix} = \mathbf{T} \begin{Bmatrix} \cos\theta_2(-\psi_I + \psi_R) - \sin\theta_1 \varphi_R \\ \sin\theta_2(\psi_I + \psi_R) + \cos\theta_1 \varphi_R \\ 0 \end{Bmatrix} \times ik_2 \tag{16}$$

The above solution is for incidence angles smaller than the critical one ($\theta_{cr} = \sin^{-1}(1/k)$).

## 3. SCATTERING BY THREE-DIMENSIONAL TOPOGRAPHIES

Consider the half-space $\Omega_h$ and the valley $\Omega_v$ (Figure 3). The displacement field related to the half-space is $\mathbf{u_h}$ and that of the valley is $\mathbf{u_v}$. The traction-free boundary condition applies on the free surface:

$$\begin{aligned} \mathbf{t}_{\mathbf{h}} &= 0 \ \text{ on } \ \Gamma_a \\ \mathbf{t}_{\mathbf{v}} &= 0 \ \text{ on } \ \Gamma_c \end{aligned} \tag{17}$$

In $\Omega_h$, the total displacement $\mathbf{u_h}$ and the total traction $\mathbf{t_h}$ are obtained by applying the principle of superposition as the sum of the free field plus the scattered field:

$$\begin{aligned} \mathbf{u}_{\mathbf{h}} &= \mathbf{u}_{\mathbf{s}} + \mathbf{u}_{\mathbf{o}} \\ \mathbf{t}_{\mathbf{h}} &= \mathbf{t}_{\mathbf{s}} + \mathbf{t}_{\mathbf{o}} \end{aligned} \tag{18}$$

where the traction $\mathbf{t_o}$ produced by the incident wave can be obtained from

$$\mathbf{t}_{\mathbf{o}} = \begin{bmatrix} [(\lambda+2\mu)\dfrac{\partial u}{\partial x} + \lambda\dfrac{\partial v}{\partial y} + \lambda\dfrac{\partial \omega}{\partial z}]n_x + \mu(\dfrac{\partial u}{\partial y} + \dfrac{\partial v}{\partial x})n_y + \mu(\dfrac{\partial u}{\partial z} + \dfrac{\partial \omega}{\partial x})n_z \\ [(\lambda+2\mu)\dfrac{\partial v}{\partial y} + \lambda\dfrac{\partial u}{\partial x} + \lambda\dfrac{\partial \omega}{\partial z}]n_y + \mu(\dfrac{\partial u}{\partial y} + \dfrac{\partial v}{\partial x})n_x + \mu(\dfrac{\partial v}{\partial z} + \dfrac{\partial \omega}{\partial y})n_z \\ [(\lambda+2\mu)\dfrac{\partial \omega}{\partial z} + \lambda\dfrac{\partial v}{\partial y} + \lambda\dfrac{\partial u}{\partial x}]n_z + \mu(\dfrac{\partial u}{\partial z} + \dfrac{\partial \omega}{\partial x})n_x + \mu(\dfrac{\partial v}{\partial z} + \dfrac{\partial \omega}{\partial y})n_y \end{bmatrix} \tag{19}$$

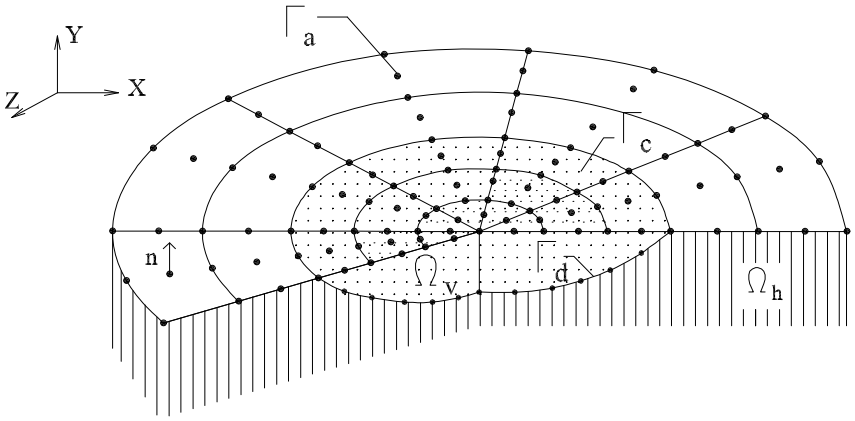


Figure 3. The half-space $\Omega_h$ and the valley $\Omega_v$

Where $n_i$ are the components of the unit outward normal to the boundary, and the displacements u, v, and ω are the components of the free field motion $\mathbf{u_o}$(u ,v ,ω), given by

the expressions (10), (13), and (16) for a harmonic wave propagating in a three-dimensional half-space. As the total traction is zero on the boundary $\Gamma_a$, the traction due to the scattered wave can be written as

$$\mathbf{t}_s = -\mathbf{t}_o \text{ on } \Gamma_a \tag{20}$$

The displacements and tractions for the half-space due to the scattered wave can be obtained from the following matrix system using the BEM

$$\mathbf{H}_h \mathbf{u}_s - \mathbf{G}_h \mathbf{t}_s = 0 \tag{21}$$

in which $\mathbf{G_h}$ and $\mathbf{H_h}$ are the influence matrices obtained from the integration of displacement and traction kernels over the boundary of the half-space, respectively. Referring to Figure 3, equation (21) can be written in the following more explicit form

$$\mathbf{H}_h [\mathbf{u}_s^a + \mathbf{u}_s^d] - \mathbf{G}_h [\mathbf{t}_s^a + \mathbf{t}_s^d] = 0 \tag{22}$$

By applying the traction free boundary condition on $\Gamma_a$, the above equation is written as

$$\mathbf{H}_h [\mathbf{u}_s^a + \mathbf{u}_s^d] - \mathbf{G}_h \mathbf{t}_s^d = -\mathbf{G}_h \mathbf{t}_o^a \tag{23}$$

where the displacements and tractions at the interface $\Gamma_d$, i.e. $\mathbf{u}_s^d$ and $\mathbf{t}_s^d$, and $\mathbf{u}_s^a$ are unknown. On the other hand, total displacements and tractions of the valley can be computed from the following system of equations using the BEM

$$\mathbf{H}_v \mathbf{u}_v - \mathbf{G}_v \mathbf{t}_v = 0 \tag{24}$$

According to Figure 3, this equation can be expressed in the following more obvious form

$$\mathbf{H}_v [\mathbf{u}_v^c + \mathbf{u}_v^d] - \mathbf{G}_v [\mathbf{t}_v^c + \mathbf{t}_v^d] = 0 \tag{25}$$

Because the total traction $\mathbf{t}_v^c = 0$, the above equation becomes

$$\mathbf{H}_v [\mathbf{u}_v^c + \mathbf{u}_v^d] - \mathbf{G}_v \mathbf{t}_v^d = 0 \tag{26}$$

Now, equation (23) for $\Omega_h$ and equation (26) for $\Omega_v$ are combined together. Compatibility and equilibrium conditions at $\Gamma_d$ are as follows

$$\begin{aligned} \mathbf{u}_v^d &= \mathbf{u}_h^d \\ \mathbf{t}_v^d &= -\mathbf{t}_h^d \end{aligned} \tag{27}$$

The total displacements and tractions on $\Gamma_d$ are given by $\mathbf{u}_h^d = \mathbf{u}_s^d + \mathbf{u}_o^d$

and $\mathbf{t}_{\mathrm{h}}^{\,d} = \mathbf{t}_{\mathrm{s}}^{\,d} + \mathbf{t}_{\mathrm{o}}^{\,d}$, respectively. Substituting these conditions into equation (26) for $\Omega_v$ yields

$$\mathbf{H}_{\mathrm{v}}\,\mathbf{u}_{\mathrm{v}}^{\,c} + \mathbf{H}_{\mathrm{v}}\,[\mathbf{u}_{\mathrm{s}}^{\,d} + \mathbf{u}_{\mathrm{o}}^{\,d}] - \mathbf{G}_{\mathrm{v}}\,[-\mathbf{t}_{\mathrm{s}}^{\,d} - \mathbf{t}_{\mathrm{o}}^{\,d}] = 0 \tag{28}$$

The resulting system from equations (23) and (28) is

$$\begin{bmatrix} \mathbf{H}_{\mathrm{h}} & \mathbf{H}_{\mathrm{h}} & 0 & -\mathbf{G}_{\mathrm{h}} \\ 0 & \mathbf{H}_{\mathrm{v}} & \mathbf{H}_{\mathrm{v}} & \mathbf{G}_{\mathrm{v}} \end{bmatrix} \begin{bmatrix} \mathbf{u}_{\mathrm{s}}^{\,a} \\ \mathbf{u}_{\mathrm{s}}^{\,d} \\ \mathbf{u}_{\mathrm{v}}^{\,c} \\ \mathbf{t}_{\mathrm{s}}^{\,d} \end{bmatrix} = \begin{bmatrix} -\mathbf{G}_{\mathrm{h}}\mathbf{t}_{\mathrm{o}}^{\,a} \\ -\mathbf{H}_{\mathrm{v}}\mathbf{u}_{\mathrm{o}}^{\,d} - \mathbf{G}_{\mathrm{v}}\mathbf{t}_{\mathrm{o}}^{\,d} \end{bmatrix} \tag{29}$$

The total displacements at the surface of the valley are obtained directly from the above equation, while the total displacements and tractions for the half-space are given by equation (18) applying the principle of superposition. Substituting the scattered values in terms of the total values into equation (29), a system of equations with unknowns of total displacements and tractions is obtained

$$\begin{bmatrix} \mathbf{H}_{\mathrm{h}} & \mathbf{H}_{\mathrm{h}} & 0 & -\mathbf{G}_{\mathrm{h}} \\ 0 & \mathbf{H}_{\mathrm{v}} & \mathbf{H}_{\mathrm{v}} & \mathbf{G}_{\mathrm{v}} \end{bmatrix} \begin{bmatrix} \mathbf{u}_{\mathrm{h}}^{\,a} \\ \mathbf{u}_{\mathrm{h}}^{\,d} \\ \mathbf{u}_{\mathrm{v}}^{\,c} \\ \mathbf{t}_{\mathrm{h}}^{\,d} \end{bmatrix} = \begin{bmatrix} \mathbf{H}_{\mathrm{h}}(\mathbf{u}_{\mathrm{o}}^{\,a} + \mathbf{u}_{\mathrm{o}}^{\,d}) - \mathbf{G}_{\mathrm{h}}(\mathbf{t}_{\mathrm{o}}^{\,a} + \mathbf{t}_{\mathrm{o}}^{\,d}) \\ 0 \end{bmatrix} \tag{30}$$

Although the system has been formulated for two regions, the half-space and the valley, the approach is general and applicable to several regions (i.e. the half-space and strata inside the valley).

## 4. COMPARISON WITH AVAILABLE SOLUTIONS IN THE LITERATURE

In order to appraise the accuracy and efficiency of the represented formulations for computing the surface displacement amplification, a number of examples are considered. The employed computer program is based on BEM in frequency domain. BEM formulations for time-harmonic elastodynamic problems have been presented by Dominguez [25] in full details.

### *4.1 Hemispherical valleys*

Responses obtained by Sanchez-Sesma [1] and Reinoso [26] for the 3D scattering of a hemispherical alluvial valley (Figure 4) due to vertical incidence of P wave has been used to test the accuracy of the present method for layer media.

The comparison of Reinoso results [26] with ours is presented in Figure 5 for the normalized frequency $\eta_{\mathrm{p}}$=0.5. The dimensionless frequency $\eta_{\mathrm{p}}$ is introduced as the ratio of the diameter of the valley and the wavelength of the incident longitudinal wave in the half-

space ($\eta_p = 2a/\lambda = \omega a/c_1\pi$), where $\omega$ is the actual frequency of the incident P wave and a is the radius of the valley. Material properties for the half space are $\mu_{hs} = \rho_{hs} = 1$ and $\nu_{hs} = .25$, and for the valley are $\mu_v = .3$, $\rho_v = .6$ and $\nu_v = .3$, where $\rho$ is the density, $\mu$ is the shear modulus, and $\nu$ is the Poisson's ratio. The shear wave velocity for the half space is equal to 1 and the longitudinal wave velocity is $\sqrt{3}$. Our results are drawn with a continuous line, while Reinoso results are drawn with filled circles.

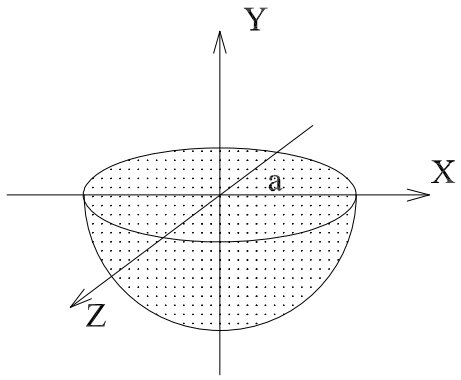


Figure 4. A hemispherical alluvial valley of radius a

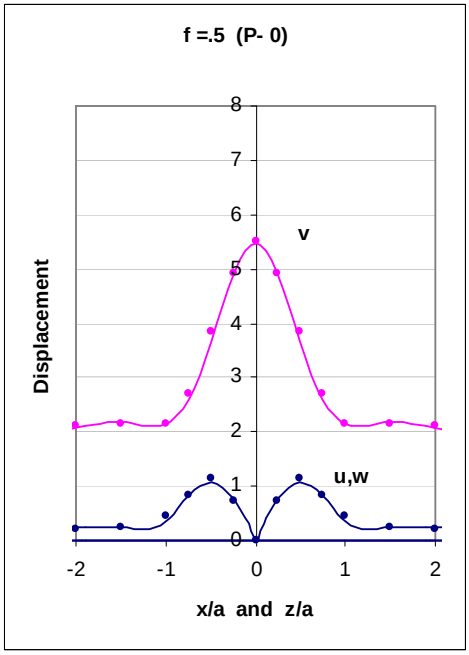


Figure 5. Amplitude of components of the surface displacement field for a hemispherical valley due to vertical incidence of P waves with normalized frequency $\eta_p$=.5

This valley is also subjected to SH wave with incidence angle of $30^\circ$ relative to the vertical axis. Material properties of the half space are similar to those of the previous one, while the properties of the valley are as follows: $\mu_v = .2025$, $\rho_v = 1$, and $\nu_v = .3$. Surface displacement amplitudes at stations along the x- and z-axes for two normalized frequencies $\eta_s = .5$ , 1 ($\eta_s = \omega\, a / c_2 \pi$) are shown in Figure 6. The dimensionless frequency $\eta_s$ is defined as the ratio of the diameter of the valley in the incident wave plane to the wavelength of the incident shear wave. The results of Sanchez-Sesma [10] are plotted with filled circles. All distances are normalized with respect to the radius of the valley. As can be seen, the comparison between both results is satisfactory.

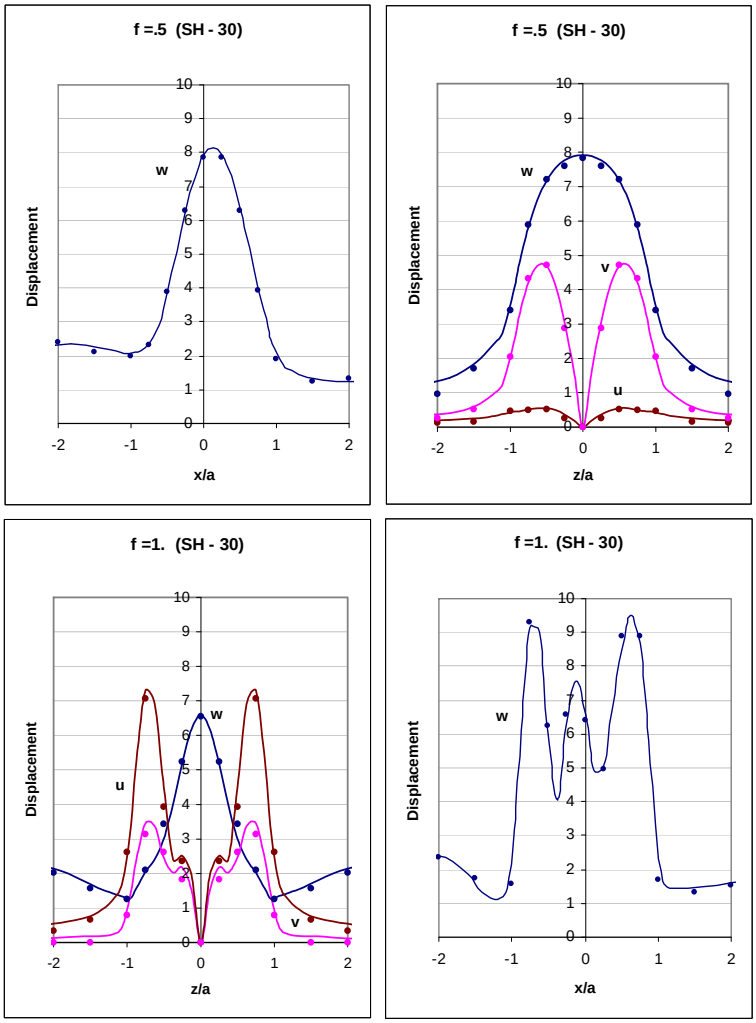


Figure 6. Amplitude of components of the surface displacement field for a hemispherical valley due to incident SH wave with incidence angle of $30^\circ$, horizontal incidence angle $0^\circ$, and normalized frequencies $\eta_s = .5$ , 1

## 5. STUDY OF SOME SURFACE TOPOGRAPHIES

In order to assess the validity of the present formulations for the computation of the surface displacement field amplification, the results were compared with other reported solutions available in the literature. A number of problems are given next.

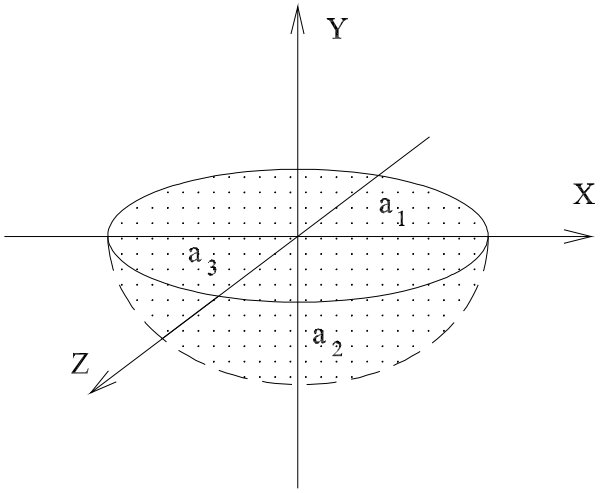


Figure 7. An elliptical-shaped alluvial valley

*5.1 Elliptical-shaped valleys*

In order to investigate the influence of the shape of the alluvial valleys on 3D scattering of waves, two elliptical-shaped valleys are considered. The equation of the semi-ellipsoid is defined by $x^2/a_1^2 + y^2/a_2^2 + z^2/a_3^2 = 1$ , $y < 0$, where $a_1$, $a_2$ and $a_3$ are the principal axes of the ellipsoid along the Cartesian coordinates x, y, and z, respectively (Figure 7). In reality, $a_1$ and $a_3$ are half of the diameters of the ellipsoid along the x- and z-directions, respectively, and $a_2$ is the depth of the valley. Results are presented for two elliptical-shaped valleys with $a_1 \neq a_2 = a_3$. All distances are normalized relative to the half-width of the valley along the z-axis (i.e. $a_3$). In addition to the actual frequency $\omega$, a dimensionless frequency $\eta_s$ is defined as the ratio of the diameter of the valley in the incident wave plane to the wavelength of the incident shear wave. The dimensions of the axes of the first valley are $a_1 = 2$ , $a_2 = a_3 = 1$ and those of the second one are $a_1 = .5$ , $a_2 = a_3 = 1$. Properties for the half space are $\mu_{hs} = \rho_{hs} = 1$ and $\nu_{hs} = .25$, and for the valley are $\mu_v = .2025$, $\rho_v = 1$, and $\nu_v = .3$. The material properties, the actual frequency of the incident wave, and the depth and width of the valleys lying in the incident wave plane are the same for both of these valleys in order to make rational comparisons. Both valleys are subjected to SH waves with incidence angles of $0^\circ$ and $30^\circ$ relative to the vertical axis y. The plane of the incident SH waves is the yz plane (horizontal incidence angle $90^\circ$). Results for the normalized frequency $\eta_s = .5$ (relative to $a_3$) are depicted by Figures 8 and 9 for the first and second valleys, respectively. The

graphs on the left-hand side correspond to the displacement field for stations along the x-axis, and the ones on the right-hand side correspond to stations along the z-axis. As expected, surface displacement field for stations along the z-axis only has one component in the x-direction. That is, the motion in the plane of the incident SH wave only occurs in the out-of-plane direction which constitutes the out-of-plane motion. However, for stations along the direction perpendicular to the plane of the incident SH wave (i.e. z-direction) all three components of the displacement field are present except for the vertical incidence which has only two in-plane components of motion. The comparative study of the responses shows that, for the narrower valley in the out-of-plane direction, a clear reduction occurs for all components of the displacement field in comparison to the other model.

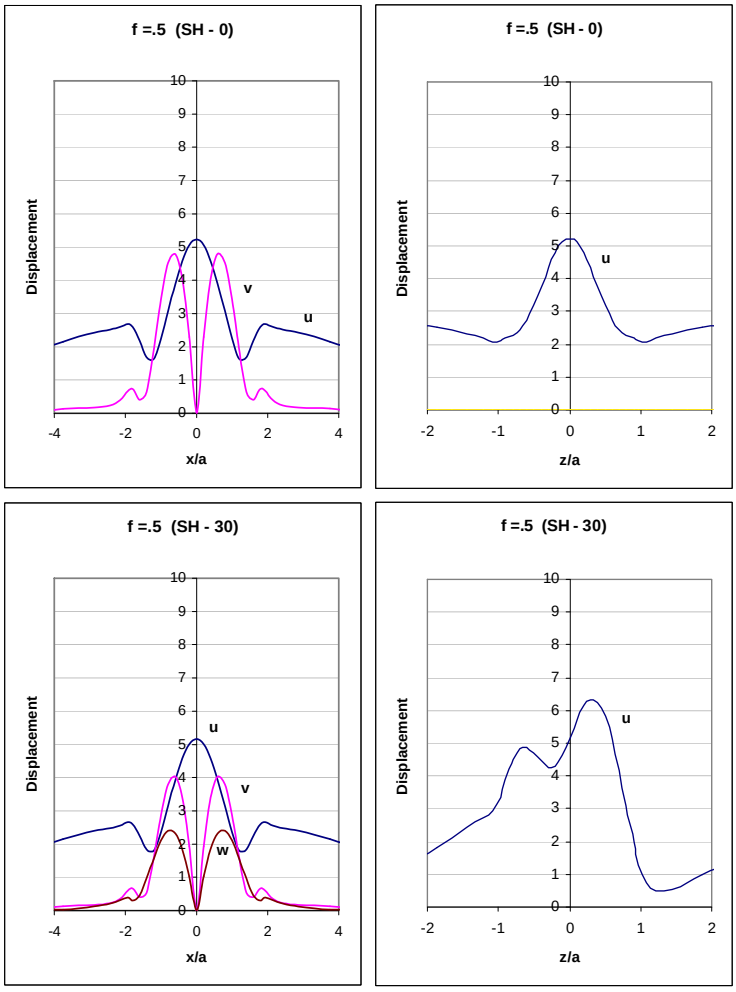


Figure 8. Amplitude of components of the surface displacement field for an elliptical-shaped valley ( $a_1 = 2$ , $a_2 = a_3 = 1$ ) due to incident SH wave with incidence angles of 0°, 30°, horizontal incidence angle $90^\circ$ , and normalized frequency $\eta_s = .5$

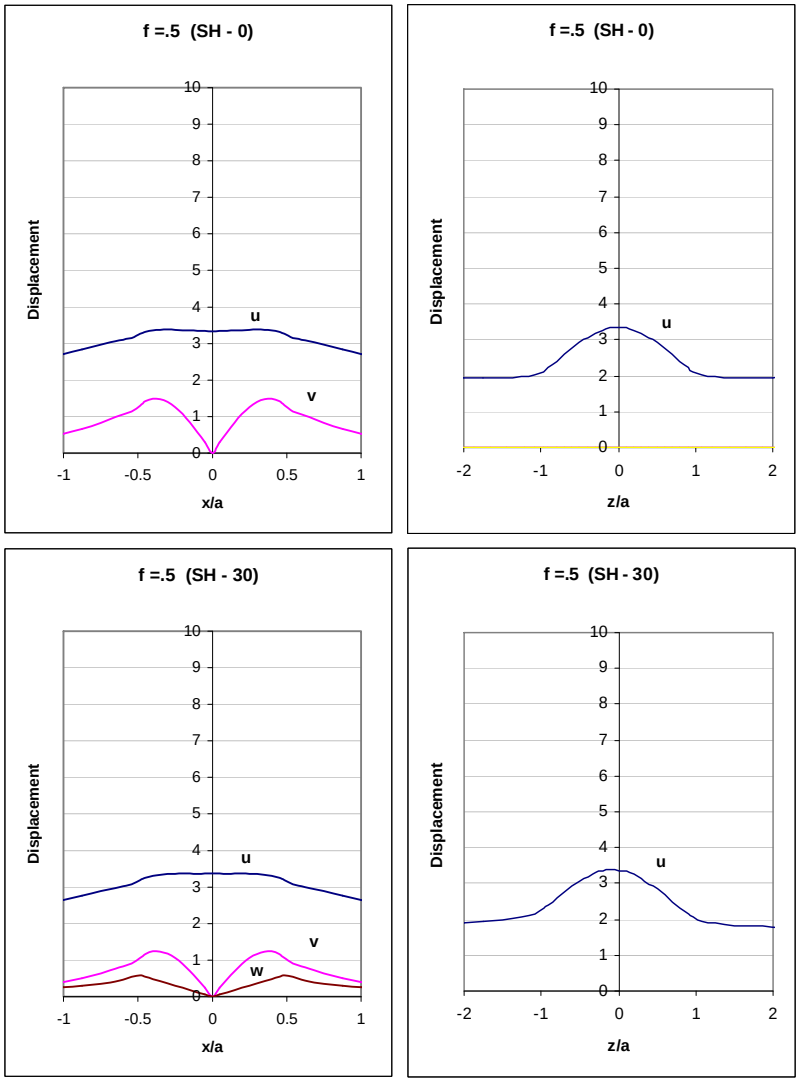


Figure 9. amplitude of components of the surface displacement field for an elliptical-shaped valley ( $a_1 = .5, a_2 = a_3 = 1$ ) due to incident SH wave with incidence angles of 0°, 30°, horizontal incidence angle 90°, and normalized frequency $\eta_s = .5$

*5.2 Hemispherical valleys with one alluvial layer*

In order to study the effect of the soil layering, surface topography, and thickness and properties of each layer on amplification potential of the site, hemispherical valleys with one alluvial layer are regarded. The internal radius of these valleys is $a = 1$, and the thickness of their alluvial layer is equal to $t$ (Figure 10). Therefore, the internal radius is the same for all these valleys, but their external radius is different which is equal to $1 + t$. Also, properties for the half space material are assumed to be the same: $\mu_{hs} = 1/3$, $\rho_{hs} = 1$, and $\nu_{hs} = .25$. These

valleys are subjected to vertical incidence of P, SH, and SV waves with azimuthal angle of incidence $0^\circ$. Results for the normalized frequency $\eta_p$=.25 (relative to a) are plotted with dotted, dashed, and solid lines for three thicknesses $t = 0.4, 0.8, 1.2$, respectively, in Figures 11 and 12.

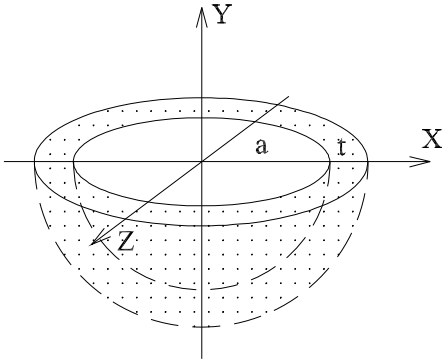


Figure 10. a hemispherical valley with one alluvial layer

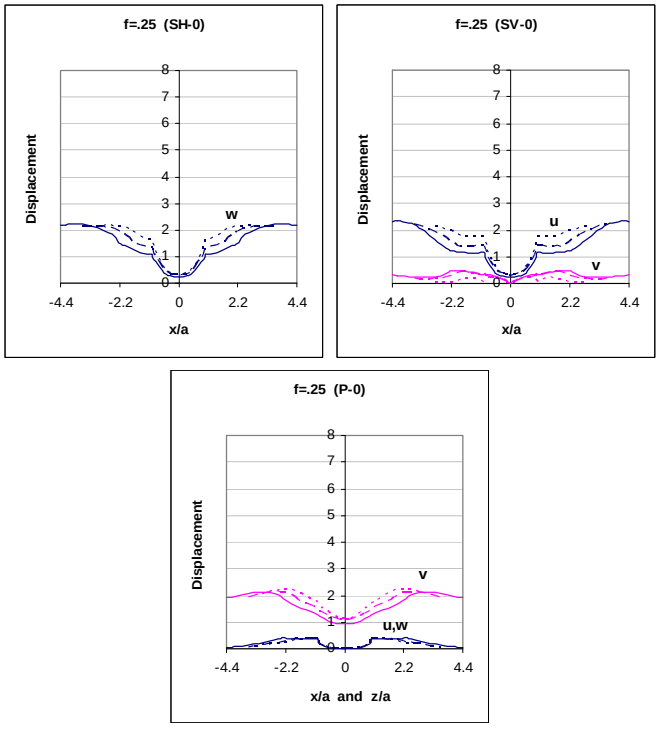


Figure 11. amplitude of components of the surface displacement field for a hemispherical valley with one alluvial layer due to vertical incidence of SH, SV, and P waves with normalized frequency $\eta_p$=.25 ( $\mu_v = \rho_v = 1$ and $\nu_v = 1/3$ ). Results are plotted with dots for $t = .4$ , with dashed lines for t=0.8, and with solid lines for t=1.2

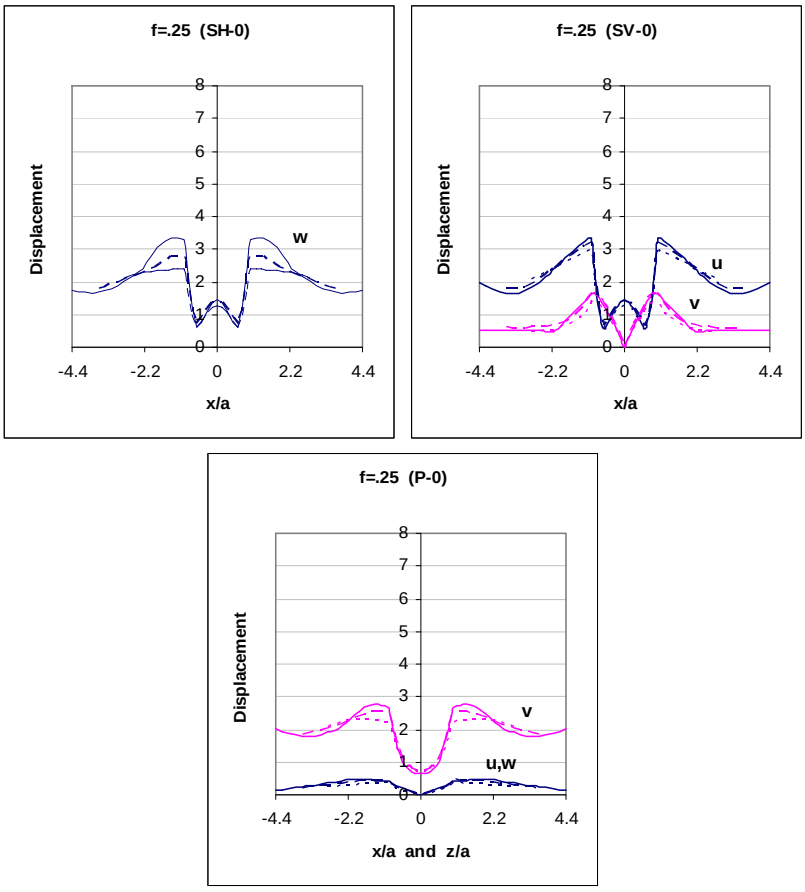


Figure 12. amplitude of components of the surface displacement field for a hemispherical valley with one alluvial layer due to vertical incidence of SH, SV, and P waves with normalized frequency $\eta_p$=.25 ( $\mu_v = .2025$ , $\rho_v = 1$ , and $v_v = .3$ ). Results are shown with dots for $t = .4$ , with dashed lines for t=.8, and with solid lines for $t = 1.2$

In the first case, material properties related to the alluvial layer are considered such that the shear wave velocity in it would be greater than that of the half space ( $\mu_v = \rho_v = 1$ and $\nu_v = 1/3$ ); the shear wave velocity in the half space is equal to 0.577, and it is equal to 1 for the alluvial layer. As can be seen, by increase of the alluvial layer thickness the amplifications decrease.

In the second case, contrary to the first one, material properties of the alluvial layer are assumed to be such that the shear wave velocity related to it would be smaller than that of the half space ( $\mu_v = .2025$ , $\rho_v = 1$ , and $\nu_v = .3$ ); accordingly, the shear wave velocity in the alluvial layer will be equal to .45. In contrast with the first state, increasing of the alluvial layer thickness produces larger amplifications.

In real, as the thickness of the alluvial layer increases, if the soil of this layer is softer

than that of the half space, i.e., if the shear wave velocity is smaller in it, the amplifications increases, and vice versa, if this layer consists of the more rigid soil than the half space, the amplifications decrease. In this respect, the more the difference between properties of the alluvial layer and the half space is, the more apparent the influence of the soil characteristics on the surface displacement field amplification is.

*5.3 Hemispherical valleys with two alluvial layers*

Again, in order to study the effect of the soil layering, and thickness and mechanical properties of each layer on the scattered displacement field, hemispherical valleys with two alluvial layers are considered. The external radius of these valleys is $a=1$, and the thickness of their first alluvial layer is equal to $t$ (Figure 13). Material properties of the half space are the same for all these valleys: $\mu_{hs}=\rho_{hs}=1$ and $\nu_{hs}=.25$. Responses of these valleys due to two angles of incidence $0^\circ$ and $30^\circ$ and horizontal angle of incidence $0^\circ$ of SH and P waves for the normalized frequency $\eta_s=.5$ (relative to a) and three thicknesses $t=0$, .2, .4 are presented in Figures 14 and 15. Results are drawn with solid lines for $t=0$, with dashed lines for $t=.2$, and with dots for $t=.4$.

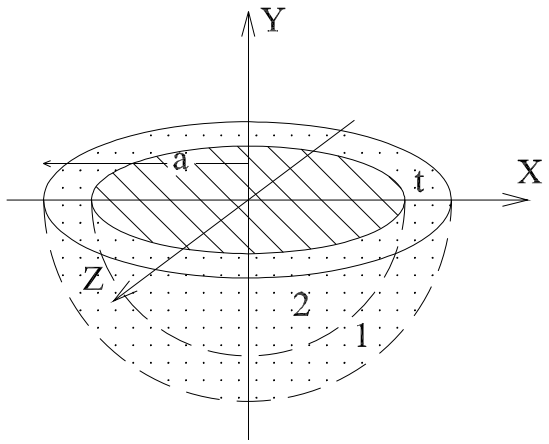


Figure 13. A hemispherical valley with two alluvial layers

In the first state, mechanical properties of the first alluvial layer are assumed to be $\mu_{v1}=\nu_{v1}=.3$ and $\rho_{v1}=.6$, and those of the second layer are taken to be $\mu_{v2}=.2025$, $\rho_{v2}=1.$, and $\nu_{v2}=.3$, where shear wave velocity for the first alluvial layer (.707) is greater than that of the second layer (.45). It is seen that by increase of the first alluvial layer thickness the amplifications decrease.

In the second state, the geological material of these two alluvial layers is exchanged with each other. Contrary to the first state, by increase of the first alluvial layer thickness larger amplitudes are observed.

Indeed, the comparative study manifests that as the thickness of the first alluvial layer increases, if the soil of this layer is softer than that of the second layer, i.e., if the shear wave

velocity is smaller in it, the surface ground motion amplifications increases, and vice versa, if this layer consists of the more rigid soil than the second layer, the amplifications decrease. In sum, it can be concluded that the larger the shear wave velocity is, the harder and safer the layer will be.

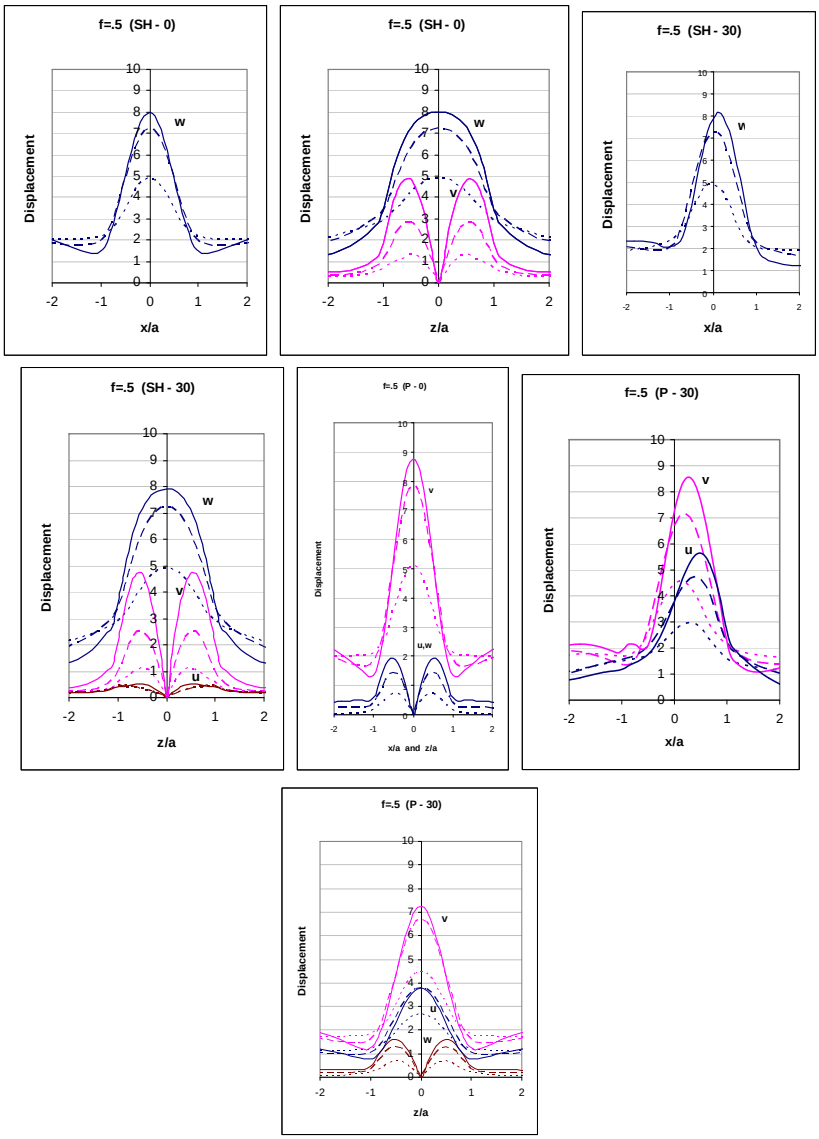


Figure 14. amplitude of components of the surface displacement field for a hemispherical valley with two alluvial layers due to incident SH and P waves with incidence angles of 0°, 30°, horizontal incidence angle 0°, and normalized frequency $\eta_s = .5$ ( $\mu_{v1} = \nu_{v1} = .3$ , $\rho_{v1} = .6$ and $\mu_{v2} = .2025$ , $\rho_{v2} = 1.$ , $\nu_{v2} = .3$ ). Results are plotted with solid, dashed, and dotted lines for three thicknesses t=0,.2, .4, respectively

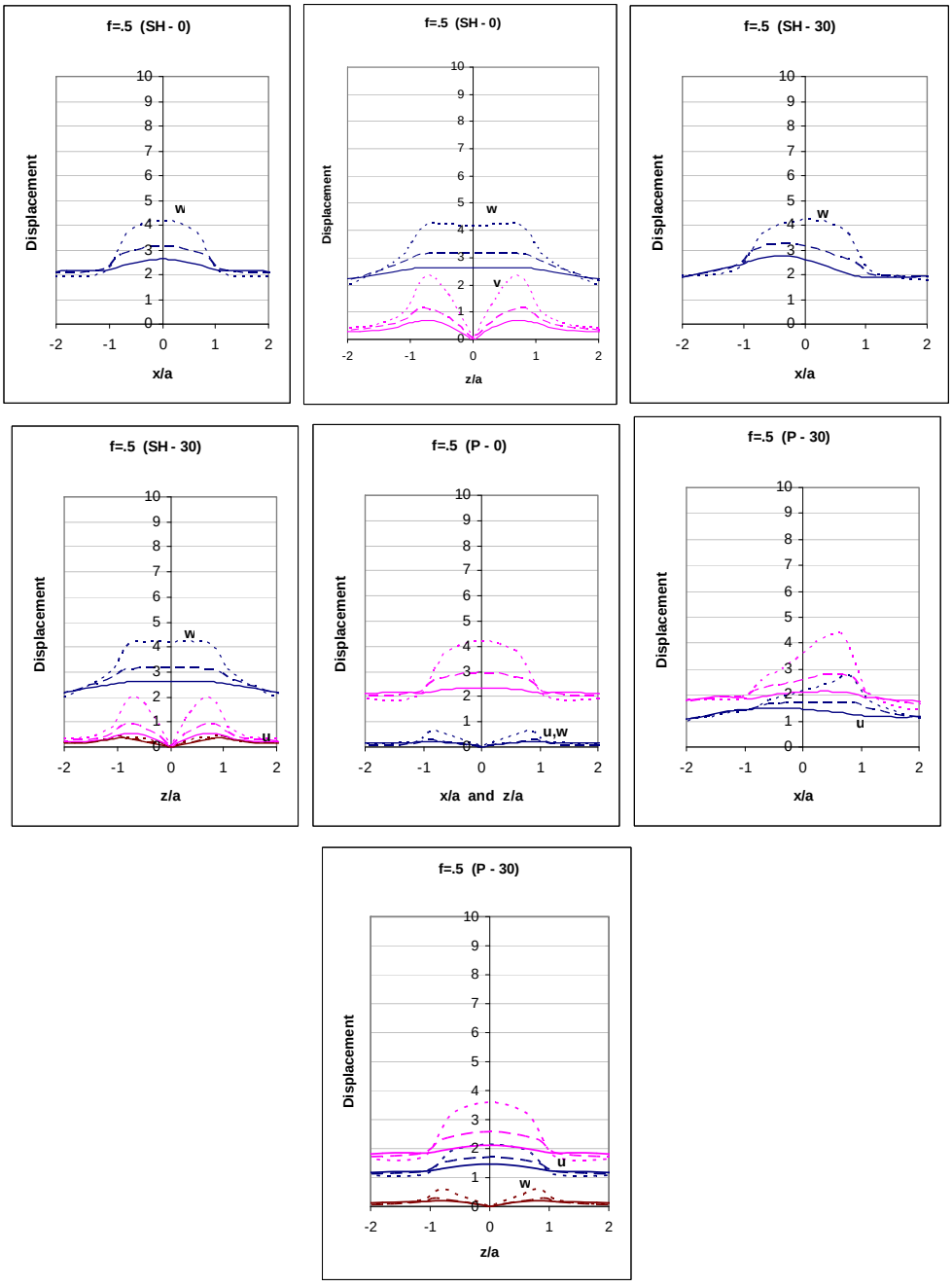


Figure 15. amplitude of components of the surface displacement field for a hemispherical valley with two alluvial layers due to incident SH and P waves with incidence angles of 0°, 30°, horizontal incidence angle 0°, and normalized frequency $\eta_s = .5$ ( $\mu_{v1} = .2025$ , $\rho_{v1} = 1.$ , $\nu_{v1} = .3$ and $\mu_{v2} = \nu_{v2} = .3$ , $\rho_{v2} = .6$ ). Results are drawn with solid, dashed, and dotted lines for three thicknesses t=0, .2, .4, respectively

## 6. CONCLUSIONS

The scattering of three-dimensional surface topographies due to incident plane harmonic SH, SV, and P waves for vertical and oblique incidences was investigated by using BEM in frequency domain. A comparative study was done to show the validity of the presented formulations. It can be realized that in incidence where the propagation wave path is perpendicular or almost perpendicular to the inclination wall, the motion tends to be more amplified than the case where incidence takes place parallel to the slope. Also, graphs are representative of amplification factor as a function of the topography coordinates. From numerical aspects of the solution, it is concluded that in order to provide acceptable convergence, as the frequency of the incident wave or its incidence angle relative to the vertical axis increases, the length of discretization over the free surface of the half space must increase as well.

One practical implication of this study is that soft layers, in which shear wave velocity is low, are prone to highly amplify the surface ground motion, while rigid layers act more safely against earthquake. Finally, it is concluded that a realistic and complete study of site effects on surface ground motion amplification requires three-dimensional modeling of irregularities. In addition, surface topography, soil layering, thickness and material properties of each layer, incident wave type, related frequency, and azimuth and angle of incidence must be considered.

## REFERENCES

1. Sanchez-Sesma FJ. Diffraction of elastic waves by three-dimensional surface irregularities, *Bulletin of the Seismological Society of America,* **73**(1983) 1621-36.
2. Lee JJ, Langston CA. Wave propagation in a three dimensional circular basin, *Bulletin of the Seismological Society of America,* **73**(1983) 1637-53.
3. Lee VW. Three-dimensional diffraction of plane P, SV and SH waves by a hemispherical alluvial valley, *Journal Soil Dynamic Earthqu Engineerng*, No. 3, **3**(1984) 133-44.
4. Eshraghi H, Dravinski M. Scattering of plane harmonic SH, SV, P and Rayleigh waves by non-axisymmetric three-dimensional canyons: as wave function expansion approach, *International Journal Earthquake Engineering Structure Dynamic*, **18**(1989) 983-98.
5. Sanchez-Sesma FJ, Perez-Rocha LE, Chavez-Perez S. Diffraction of elastic waves by three-dimensional surface irregularities: Part II, *Bulletin of the Seismological Society of America*, **79**(1989) 101- 12.
6. Sanchez-Sesma FJ, Perez-Rocha LE, Reinoso E. Ground motion in Mexico City during the April 25, 1989, *Guerrero earthquake*. *Teetonophysics*, **218**(1993) 127-40.
7. Luco JE, Wong HL, De Barros FC. Three dimensional response of a cylindrical canyon in a layered half-space, *Earthquake Engineering & Structural Dynamics*, **19**(1990) 799-817.
8. Zhang L, Chopra AK. Three-dimensional analysis of spatially varying ground motions around a uniform canyon in a homogeneous half-space, *Earthquake Engineering and*

*Structural Dynamic*s, **20**(1991) 911-26.
9. Khair KR, Datta SK, Shah AH. Amplification of obliquely incident seismic waves by cylindrical alluvial valleys of arbitrary cross-sectional shape, Part I. Incident P and SV waves, *Bulletin of the Seismological Society of America*, **79**(1989) 610-30.
10. Khair KR, Datta SK, Shah AH. Amplification of obliquely incident seismic waves by cylindrical alluvial valleys of arbitrary cross-sectional shape, Part II. Incident SH and Rayleigh waves, *Bulletin of the Seismological Society of America*, **81**(1991) 346-57.
11. Liu SW, Datta SK, Bouden M, Shah AH. Scattering of obliquely incident seismic waves by a cylindrical valley in a layered half-space, *Earthquake Engineering and Structural Dynamics*, **20**(1991) 859-70.
12. Yomogida K, Etgen JT. 3-D wave propagation in the Los Angeles basin for the Whittier-Narrows earthquakes. *Bulletin of the Seismological Society of America*, **83** (1993) 1325-41.
13. Hizada Y, Aki K, Teng T. 3-D simulations of surface wave propagation in the Kanto sedimentary basin, Japan. Part 2: Application of the surface wave BEM. *Bulletin of the Seismological Society of America*, **83**(1993) 1700-20.
14. Sanchez-Sesma FJ, Luzon F. Seismic response of three-dimensional alluvial valleys for incident P, S and Rayleigh waves, *Bulletin of the Seismological Society of America*, **85**(1995) 269–84.
15. Pedersen HA, Campillo M, Sanchez-Sesma FJ. Azimuth-dependent wave amplification in alluvial valleys. *Soil Dynamics and Earthquake Engineering,* **14**(1995) 289–300.
16. DeBarros FCP, Luco JE. Amplification of oblique incident waves by a cylindrical valley embedded in a layered half-space, *Soil Dynamics and Earthquake Engineering,* **14**(1995) 163-75.
17. Dravinski M, Mossessian TK. Scattering of plane harmonic waves by multiple dipping layers of arbitrary shape, in: A.S. Cakmak, ed., *Ground Motion and Engineering Seismology*, Elsevier, Amsterdam, 1987, pp. 91-105.
18. Mossessian TK, Dravinski M. Scattering of elastic waves by three-dimensional surface topographies. *Wave motion*, North-Holland, **11**(1989) 579-92.
19. Reinoso E, Wrobel LC, Power H. Three-dimensional scattering of seismic waves from topographical structures, *Soil Dynamics and Earthquake Engineering*, **16**(1996) 41-61.
20. Mohammadnejad T. 3D study of topographic effect on amplification of earthquake waves. M.Sc. Dissertation, *Faculty of Engineering*, University of Tehran, 2005.
21. Gatmiri B, Arson C. Nguyen KV. Seismic site effects by an optimized 2D BE/FE method I. Theory, numerical optimization and application to topographical irregularities. *Soil Dynamics and Earthquake Engineering*, **28**(2007) 632-45.
22. Gatmiri B, Arson C. Seismic site effects by an optimized 2D BE/FE method II.Quantification of site effects in two-dimensional sedimentary valleys, *Soil Dynamics and Earthquake Engineering,* **28**(2007) 646-61.
23. Lee Sh J, Komatitsch D, Huang B Sh, Tromp J. Effects of Topography on Seismic-Wave Propagation: An Example from Northern Taiwan. *Bulletin of the Seismological Society of America*, No. 1, **99**(2009) 314-25.
24. Rahimian M, Omidvar B, Derakhshan H, Noorzad A. Effects of arbitrary shaped surface topographies on earthquake ground motion using boundary element method in

time domain. *Iranian Journal of Science & Technology*, *Transaction B, Engineering*, No. B5, **31**(2007) 473-85.
25. Dominguez J. *Boundary Elements in Dynamics*, Computational Mechanics Publications, 1993.
26. Reinoso E. *Scattering of Seismic Waves: Applications to the Mexico City Valley*, WIT Press, London, 2002.